AIMS Materials Science, 7(6): 836–858.
DOI: 10.3934/matersci.2020.6.836
Received: 31 August 2020
Accepted: 20 November 2020
Published: 03 December 2020

http://www.aimspress.com/journal/Materials

Review

Shape memory alloy heat activation: State of the art review

Abdelmoneim El Naggar and Maged A. Youssef*

Civil and Environmental Engineering, Western University, London, ON, N6A 5B9, Canada

* **Correspondence:** Email: youssef@uwo.ca; Tel: +15196612111, 88661.

Abstract: The use of shape memory alloys (SMAs) in civil structures attracted the attention of researchers worldwide. This interest is due the unique properties of SMAs, the shape memory effect (SME) and pseudoelasticity. Other desirable attributes for SMA include biocompatibility, high specific strength, wear resistance, anti-fatigue characteristics, and high yield strength. These beneficial qualities allow for a wide range of applications ranging from aerospace field to the medical and civil engineering fields. To intelligently utilize shape memory alloys and widen their application potential, certain characteristics including the heat activation and heat transfer mechanisms must be thoroughly understood. Such understanding would allow the development and optimization of systems utilizing SMA. Hence, this paper presents a state-of-the-art review about shape memory alloys with specific focus on the heat activation mechanisms and the heat transfer modes.

Keywords: shape memory alloys; pseudoelasticity; shape memory effect; rapid pulse activation; convective heat transfer; conduction

1. Introduction

Shape memory alloy is a multifunctional active material, which can exhibit sensing and actuation capabilities. It has been on the forefront of research, especially in the last two decades. The two outstanding properties that set SMA apart from any other material are the shape memory effect and superelasticity. Returning to the original material shape after deformation through heating is referred to as the shape memory effect (SME), while superelasticity refers to the material's ability to resist large cyclic deformations without acquiring any residual stresses. These unique properties allow for many potential applications in civil structures. SMA also possesses superior mechanical

energy absorption and dissipation abilities, which open a wide range of applications in vibration control, damping, and energy dissipation.

The purpose of this paper is to provide the necessary information for future use of the SME property in civil structures. The paper starts by providing general information about SMA, applications and limitations. Then, a discussion about the available heat activation methods to achieve SME and the heat transfer during the activation stage are presented.

2. SMA material characteristics

SMAs have two different phases responsible for the shape recovery phenomena. A high temperature parent phase (austenite) and a low temperature product phase (martensite). While, the austenite phase has a cubic crystal structure, the martensite phase structure is usually tetragonal, orthorhombic, or monoclinic. The transformation between these structures occurs through the shear lattice distortion, and the transformation is known as a martensitic transformation [1]. The martensitic crystals formed can have different orientations or variants. These variants can exist in two forms: twinned and detwinned.

The reversible solid-solid phase transformation between austenite and martensite forms the basis of the SMA's unique performance. During the forward transformation from austenite to martensite, in the absence of any externally applied loading, austenite begins to transform to twinned martensite at the martensitic start temperature (M_s). The transformation to the fully twinned martensitic phase is completed at the martensitic finish temperature (M_f). If sufficient heat is applied and the austenitic start temperature (A_s) is reached, the reverse transformation from martensite back to austenite could be initiated, and the crystal structure would transform completely back to austenite at the austenitic finish temperature (A_f).

A typical stress-strain-temperature diagram exhibiting the SME is shown in Figure 1. The two unique behaviors exhibited by SMA are the shape memory effect (SME) and the Pseudoelasticity (PE). If the temperature is below A_s, SMA deforms under loading and its structure changes from the twinned martensite to detwinned martensite, which results in residual strains upon unloading. Heating the SMA above A_f allows the SMA to transform back into the parent austenite phase and regain its original shape. This process is called the SME. In other words, SME occurs when the original shape of the SMA is recovered after heat is applied.

Another unique phenomenon is the pseudoelastic effect (PE), which occurs when the temperature of the SMA material is above the A_f, and a complete shape recovery is observed upon unloading to austenite. In other words, SMA exhibits a pseudoelastic response and develops a superelastic hysteric behavior when loaded at high temperatures. A typical SMA loading path and cycle for PE behavior is shown in the Figure 2.

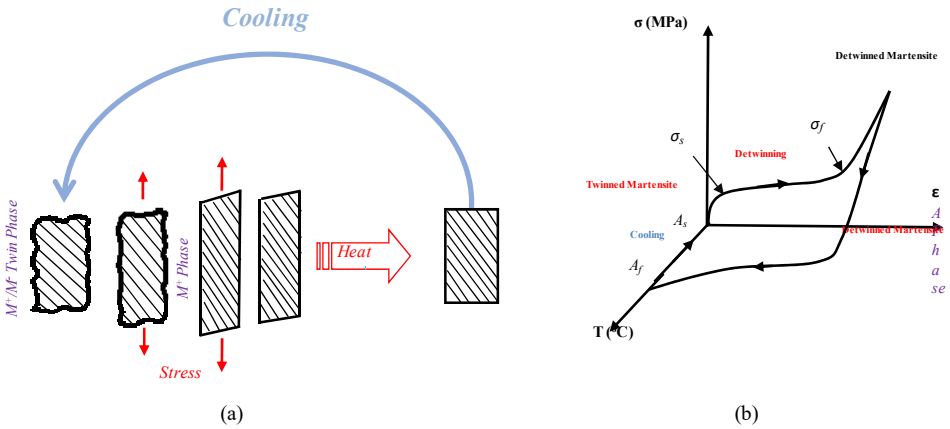

Figure 1. Transformation of SMA in response to temperature and loading. (a) Phase change in response to heating, cooling, and stressing, (b) Typical stress strain temperature data for SME.

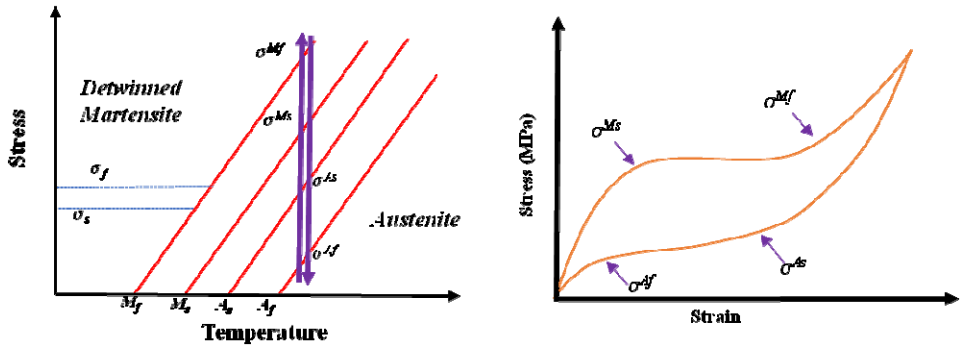

Figure 2. Pseudoelastic loading.

3. Current SMA applications

SMA is of great interest and use in the biomedical engineering and aerospace fields due to its biocompatibility and corrosion resistant properties. The material's passive properties make it attractive for non-intrusive surgical techniques, such as cardiac ablation, catheter in vivo steering, and heart valves [2–7]. Similarly, the aerospace industry makes great use of SMA actuator systems, largely due to the high force to mass ratio. For instance, SMA is used to actuate a variable area chevron to improve the jet outlet efficiency [4,8,9]. Costanza and Tata [10] described how the variable geometry chevron actuated by SMA has been developed for its thrust, reduced noise, and general efficiency optimization. SMA space applications have been beneficial for isolating the micro-vibrations, for low-shock release devices and self-deployable solar sails.

As a smart material that can be utilized in civil structures to dissipate seismic energy and provide self-centering capabilities, SMA material has proven to enhance the dynamic performance and member longevity. Indeed, SMA based bracing systems have drawn great research attention over the past two decades as a feasible method to enhance seismic performance of civil structures. Such applications rely on the SMA's pseudoelastic phenomena. Research efforts have included

numerically investigating the performance of SMA braced frames by assuming that the brace consists of short SMA elements connected to rigid segments. SMA frame configurations have been experimentally and analytically tested and proven to be feasible with beneficial resistance and energy dissipation properties, holding great potential to save billions of dollars' worth of maintenance and seismic remedy efforts [11–14].

Many structures have already made use of SMA as a rehabilitation material. For example, after suffering significant damage to the bell tower due to a 4.8 Richter magnitude earthquake on October 15, 1996, the St. Giorgio Church, located in Trignano, Italy, was rehabilitated using SMAs. Steel tie bars with SMA devices were placed in the internal corners of the bell towers to increase its flexural resistance [15]. Likewise, the Basilica of St. Francesco, in Assisi, Italy, was heavily damaged from an earthquake in 1997. The main challenge to its restoration was to rectify its structural capacity, while maintaining the original concept of the structure. To reduce the seismic forces transferred to the tympanum, a connection was created using a superelastic SMA material that demonstrates structural properties for different horizontal forces [16,17].

Similarly, SME behavior makes SMA material very promising in concrete healing and structural strengthening. By prestressing the SMA in martensitic state, then applying heat to trigger the SME, a contraction of the material occurs. Hence, a concrete column wrapped with prestressed SMA wires would provide the column with the needed confinement to increase its structural capacity and enhance its behavior under extensive loading. The high recovery stress associated with the shape recovery of SMAs was utilized as a relatively simple and reliable technique to apply external active confining pressure on RC bridge columns to improve their ductility, as shown in Figure 3 [18–20]. Hence, this retrofitting configuration has great potential within the structural rehabilitation and resistance field.

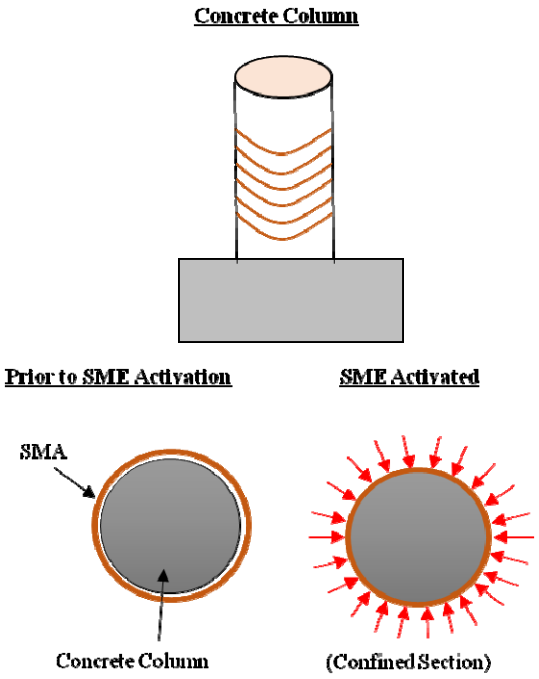

Figure 3. Schematic illustration of the concept of using prestrained SMA hoops to apply external confining pressure on RC bridge columns.

4. SMA limitations

Practical challenges have hindered many of the SMA potential applications. Strain change actuation of the SMA material involves a intrinsic energy loss due to latent heat, resulting in a non-conservative activation. The SMA wires may also be susceptible to a coupled thermo-mechanical interaction with the surroundings. This makes the SMA compartment acts as a heat sink causing inhomogeneity in surface temperature, and eventually, a phase fraction distribution within the wire [21].

As previously mentioned, SMA material properties are heavily dependent on the ambient temperature. Due to the thermo mechanical nature of the SMAs, an increase in temperature is followed by a decrease in stress, which results in larger stresses being required for the forward transformation. Forward and reverse phase transformation processes are affected differently by such changes, and so are the behavior specifics of the material. This includes the area of the developed hysteresis and therefore the energy dissipation properties of the SMA material, which have a direct effect on the SME and the pseudoelasticity phenomena, possibly compromising the materials unique behavior.

Furthermore, even though the large strain and work output are promising characteristic of SMA activation, the SME process is considered slow due to the required activation time and the cooling rate. The following section provides a state-of-the-art review regarding the different SME activation techniques and an overview of the mechanical response under these techniques. Also, a review regarding the heat transfer mechanisms is conducted to give a better sense of how manipulating the transient heat transfer method could optimize the overall system's performance.

5. SME electro-resistive activation methods

5.1. Conventional activation

Conventional resistive electric heating approaches trigger the SME by applying a small voltage to heat up the SMA. The magnitude of the applied voltage is determined based on the SMA resistivity. The amount of the current passing through the SMA, which eventually results in the heating up of the material to the desired actuating temperature, needs to be defined. Conventional actuation methods usually utilize simple technology, which often result in a slower activation process, taking as long as several minutes to activate the SME, depending on the power supplied, electrical resistance, and the material transformation temperatures.

A major drawback of conventional activation is that the process is relatively slow, and major heat transfer between the SMA and the ambient environment usually occurs. This lost heat could get transferred to certain structural elements when used for retrofitting purposes, which could be harmful to the overall structural capacity. For example, during retrofitting of a beam element, if the heat supposed to activate the SME and enhance the beam's capacity, got transferred to the beam, it will result in the development of thermal expansion forces. These forces can oppose the contraction of the SMA material due to the SME, thereby, compromising the SMA's rehabilitation potential and decreasing the material's practicality.

5.2. Rapid pulse activation

The first SMA pulse activation study utilized kilovolt pulses with durations of microseconds to activate the SME, while acquiring the same frequency response, displacement, and SMA force, focusing on the kinetic of the nickel titanium phase transformation. High voltage activation of SMA generates instantaneous forces, leading to a highly dynamic stroke due to the high accelerations and velocities. SMA wire geometric characteristics such as wire length and diameter change due to the contraction byproduct of the SME, along with other properties like phase composition and temperature. Since, these properties affect the wire's electrical resistance, and subsequently, the desired activation voltage, varying the electrical current would be necessary to supply a constant applied voltage. A rapid heating pulse can be achieved by discharging several capacitors across the SMA wire, depending on the desired voltage. Assuming a simple RC circuit, the characteristic discharge time τ would be determined by Eq 1. This discharge time should be shorter than the characteristic response time of the SMA wire. Likewise, the resistance of the wire is directly related to its length, L_0, through Eq 2. Using this information, the penetration depth, d, of the electric pulse applied can be determined through Eq 3. The penetration depth, d, must exceed the wire radius, r, to ensure a uniform heating of the wire. Hence, the maximum radius an SMA wire can be determined using Eq 4.

$$\tau = RC \tag{1}$$

where R is the resistance and C is the capacitance.

$$R = \frac{\rho_e L_0}{\pi r^2} \tag{2}$$

where r is the wire's radius and ρ_e is the wire's resistivity.

$$d = \sqrt{\frac{2\rho_e \tau}{\mu}} \tag{3}$$

where μ is the magnetic permeability of SMA.

$$r_{max} = \sqrt{\frac{2\rho_e t_0}{\mu}} \tag{4}$$

Using the above equations, Vollach and Shilo [22] developed an experimental general circuit design, to accommodate for the rapid heating of the SMA. The capabilities of a fast one directional actuation mode based on one occasional rapid joule heating was explored. They developed a unique experimental system that applied a high voltage electric pulse, tuned to produce a variable temperature jump of up to 160 ^{o}C within few microseconds to a 0.2 mm wide detwinned NiTi wire and measured the resulting displacement due to this phase transformation. The experimental setup, shown in Figure 4, consisted of a wire clamped to a fixed bridge from one end, and connected to a movable rod at the other end, where the displacement is monitored by an optical encoder that measures the displacement of the grating device and a laser doppler vibrometer.

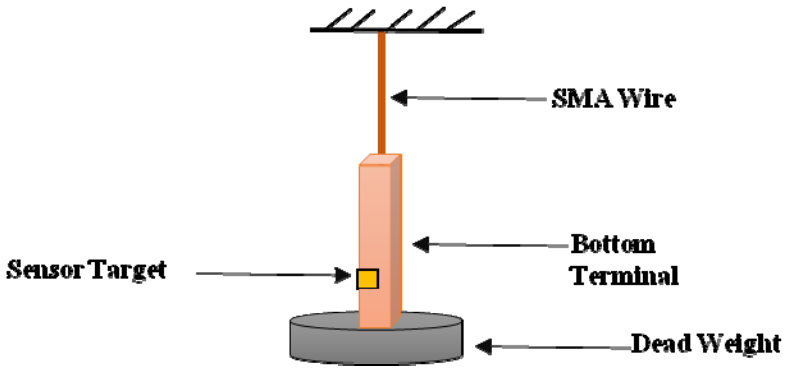

Figure 4. Vollach et al.'s [22] mechanical setup.

The experimental results indicated that a dead time delay exists between the electric pulse and the wire's response. This dead time exists due to the austenite nucleation time, and it imposed a limit on the fastest possible shape memory actuation. In addition, a relationship between the dead weight and the average acceleration and maximum velocity was discovered. The maximal velocity correlated to a constant kinetic energy delivered by the wire, which means there is a constant integrand over the stress strain curve regardless of the dead weight. The relationship between the maximal velocity and the maximal kinetic energy is given by Eq 5.

$$v^{max} = \sqrt{\frac{2E_K max}{m}} v \tag{5}$$

where m is the mass, $E_K max$ is the maximal kinetic energy, and v^{max} is the maximum velocity.

By incorporating the measurements of the generated force and displacement as a function of time with full field and IR photography, Vollach et al. [23] were able to further investigate the mechanical response of the SMA wires under rapid actuation and revealed several unique dynamic effects. A block diagram of the experimental setup is shown in Figure 5. After utilizing a 5 kV, it was observed that 99% of the energy is transferred to the 0.2 mm wide wire after about 4 ms and that a duration of microseconds was sufficient to fully penetrate the wire, heating it uniformly. Different pulse energies were used for the activation process, but the discharge time was similar. Figure 6 shows the different variables for a typical heating pulse used. This investigation allowed a direct study of the dead time, defined as the duration between the end of the electric pulse and the onset of the stress rise. This revealed that the main contribution to the dead time comes from the response of the material itself.

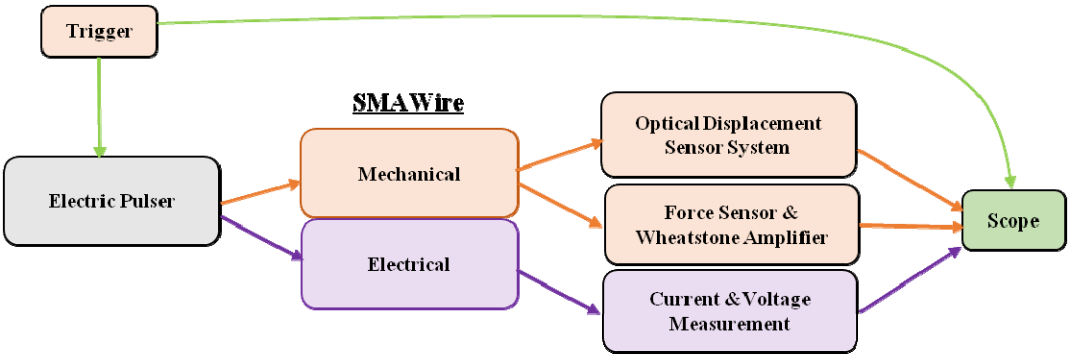

Figure 5. A block diagram of Vollach et al.'s [23] experimental setup.

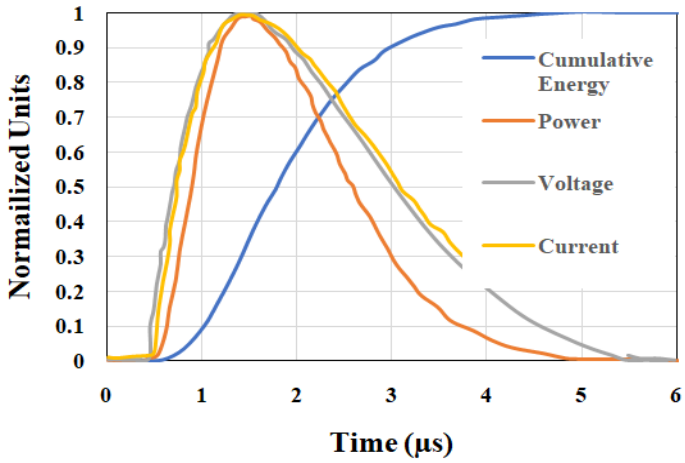

Figure 6. A plot of the different variables of a typical heating pulse.

After realizing that the slow response time of SMA actuators is attributed to the slower rate of heat transfer rather than being limited based on the rate of phase transformation, Malka and Shilo [24] developed a pulse heating SMA actuator aimed to overcome this drawback and enhance the energy efficiency of the system. A detailed depiction of his setup is shown in Figure 7. Eq 6 was used to determine the necessary temperature to reach the wire's given transition stress. Likewise, Malka and Shilo [24] derived Eq 7 to determine the input energy per unit volume required for heating the SMA wire and inducing the phase transformation, U_{in}.

$$\sigma \cong \frac{H}{T_0 \varepsilon_0}(T - T_0) \tag{6}$$

where H and T_0 are the latent heat and transition temperature of the phase equation, σ and ε_0 are the initial pre-elongation (detwinning) stress and strain of the martensite.

$$U_{\text{in}} = \left[C_p(T_0 - T_{\text{R}}) + H\right] + Q + \frac{C_p T_0}{H} U_{\text{out}} \tag{7}$$

where C_p is the heat capacitance of the SMA, T_{R} is the room temperature, and Q is the wasted heat that is passed from the SMA to its surrounding during heating and phase transformation.

One of the advantages of rapid heating is that as the heating time decreases the input energy,U_{in}, proving rapid heating as a more efficient mechanism to SMA activation. This energetic efficiency increases as the stress in the SMA wire increases.The above equation determined the input energy required to be transferred to the wires by a set of capacitors. This information was then used to determine the adequate circuit design for the SMA activating system through Eq 8.

$$E_{\text{in}} = \eta \cdot \frac{1}{2} C V^2 \tag{8}$$

where $\eta = \frac{R}{R+R_p}$, E_{in} is the input energy required, C is the overall capacitance, V is the charged voltage, and η is an efficiency coefficient, where R is the overall resistance of the SMA, and R_P is the parasitic resistance due to the resistance of the electric wire connections between the capacitors and the SMAs.

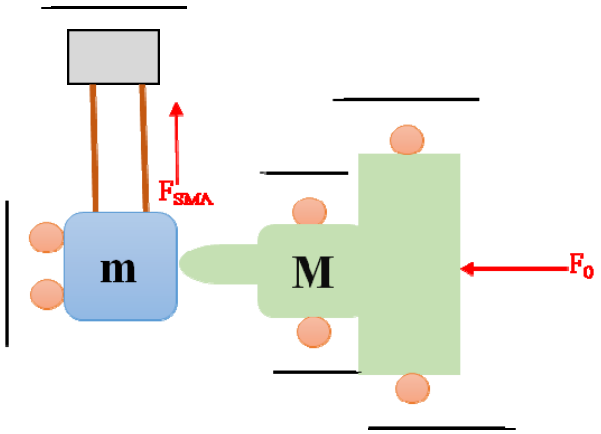

Figure 7. A detailed illustration of Malka and Shilo's [24] experimental setup.

Motzki et al. [25] investigated fast and energy efficient actuation strategies, based on short pulses in the millisecond ranges, to improve the performance of the SMA wire actuators. They varied the pulse width and realized that the use of higher voltages leads to a highly dynamic activation process, unlike the conventional low voltage quasi static activation processes. Reference measurements for the conventional SMA actuation process are shown in Figure 8. The energy balance for this conventional activation was described by Eq 9. Contrary to this conventional activation, it was determined that rapid heat activation eliminates heat loss to the environment, and hence its energy balance can be reduced to Eq 10.

$$\int_{t_0}^{t_1} V \cdot i \cdot dt = m_{\text{SMA}} \cdot c \cdot (T_{\text{trans}} - T_{\text{env}}) + h \cdot m_{\text{SMA}} - \int_{t_0}^{t_1} \alpha \cdot A_{\text{SMA}} \cdot (T_{\text{SMA}}(t) - T_{\text{env}}) \cdot dt \tag{9}$$

where the electrical energy input is determined by calculating the electrical power, P, which is a product of the voltage, V, and the current, i. t_0 is the initial time and t_1 is the time at which the transformation temperature T_{trans} is reached and the phase transformation is achieved. T_{env} represents the room temperature, c is the specific heat capacity, m_{SMA} is the mass of the SMA

material, and $h \cdot m_{\mathrm{SMA}}$ is the latent heat of phase transformation. The last term accounts for the heat between the SMA material and the environment, where α is the convective cooling coefficient, A_{SMA} is the SMA material's surface area, and $T_{\mathrm{SMA}}(t)$ is the temperature of the SMA material at time, t.

$$U \cdot i \cdot (t_1 - t_0) = m_{\mathrm{SMA}} \cdot c \cdot (T_{\mathrm{trans}} - T_{\mathrm{env}}) + h \cdot m_{\mathrm{SMA}} \tag{10}$$

The input energy for the measurements, shown in Figure 8, were much lower than the input energy for the conventional activation. This energy conservation will be discussed in more detail in section SMA limitations. Figure 8 shows the results of SMA higher voltage activation, in contrast to the slower conventional activation, with the same 0.076 mm wide SMA wire. The current signal from the higher voltage activation processes are similar to the conventional current in the sense that the current slightly decreases due to the rising temperature and rising electrical resistance, but once the contraction begins due to the phase transformation, the SMA wire gets shorter and the diameter increases, leading to a drop in the wire electrical resistance allowing a noticeable increase in the electric current running through the SMA wire. The higher supply voltages of 48 V and 125 V result in a faster temperature increase, leading to a more significant decrease in the current signal.

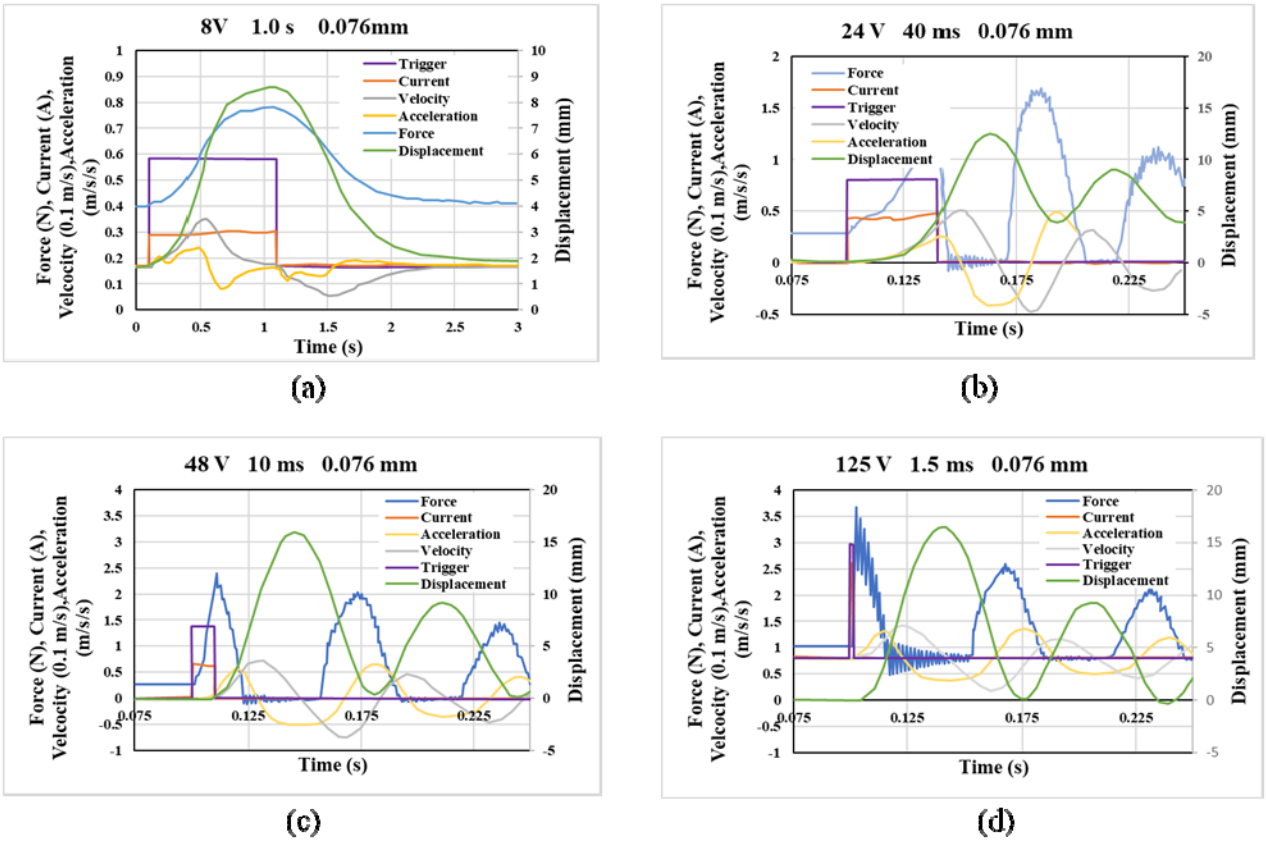

Figure 8. SMA activation measurements on a 0.076 mm wide SMA wire. (a) Conventional 8V activation for 1 s, (b) 24 V activation for 40 ms, (c) 48 V activation for 10 ms, and (d) 125 V activation for 1.5 ms.

Similarly, increasing the activation pulse time increased the generated force due to the increased energy input allowing more of the SMA material to undergo phase transformation. Even though the

time to reach the maximum stroke increased due to the increased displacement, the average mass speed due to the wire contraction was much higher for the longer activation pulses. Furthermore, the effect of SMA wire diameter on the performance of the SMA material during rapid activation was investigated. A larger SMA wire diameter resulted in a lower electrical resistance, as expected due to inverse relationship between wire's radius and resistance as shown in Eq 2. This reduced electrical resistance resulted in a higher generated power during activation at a constant voltage. Figure 9 shows the effect of SMA wire diameter on the generated force. The experiment ran at a supply voltage of 48 V and initial load of 0.28 N.

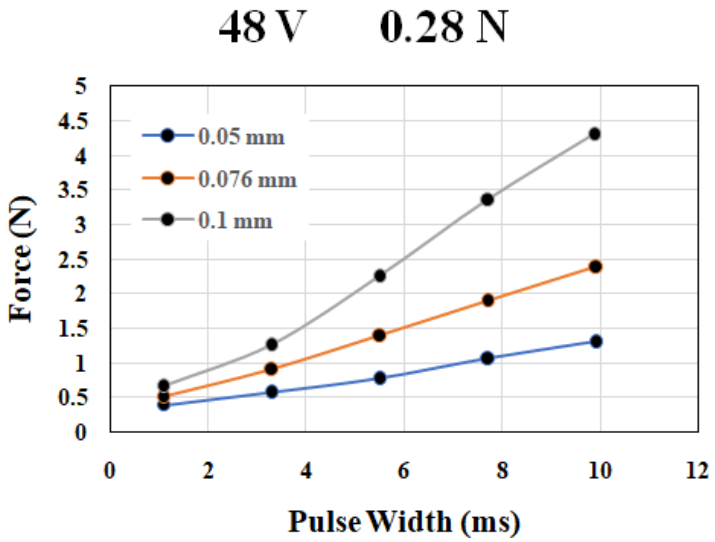

Figure 9. A comparison of the maximum force for different SMA wire diameters.

The total energy input at defined pulse lengths was higher for larger diameters, resulting in greater energy utilized for phase transformation, allowing the generation of higher contraction forces. Higher contraction forces would lead to greater strokes and faster accelerations, reaching the maximum displacements at a shorter time. Finally, the effect of different voltage levels on the performance of the SMA material during phase transformation was studied. To ensure that the input energy does not change, the activation pulse length was adjusted, while the diameter (0.0076 mm) was kept the same. As shown in Figure 10, a higher voltage resulted in a higher force at a lower input energy level. At 24 V, the SMA wire was not able to generate the same stroke compared to the other voltage levels. Furthermore, the activation pulses were much longer, which resulted in cooling the wire during the activation process. The activation pulse at 0.4 J was 40 ms long, a time interval long enough to allow the system to reach thermodynamic equilibrium and result in lower forces generated. For 125 V, the energy input of 0.4 J reached the referenced displacement in under 22 ms.

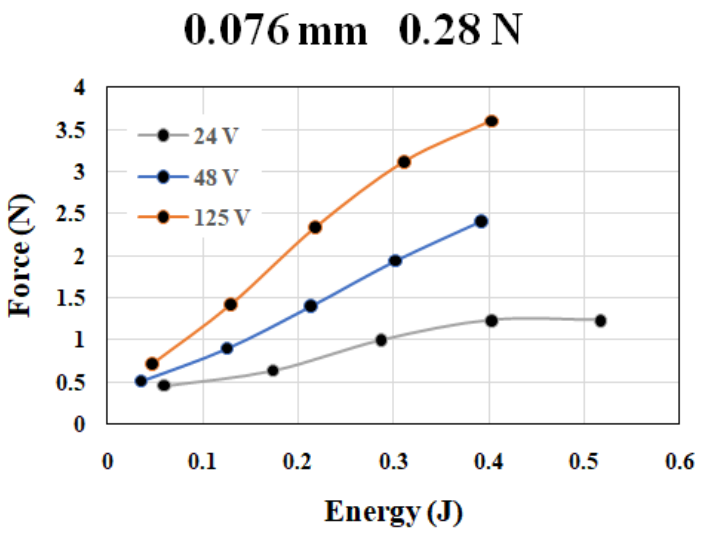

Figure 10. A comparison of the maximum force for different voltage supplies.

6. Activation energy efficiency

Most conventional quasi-static activation approaches heat SMA wires through electric currents varying from zero to four ampere depending on the SMA material properties and volume. Unfortunately, the low voltage activation of SMA wires puts the activation process in non-adiabatic conditions where large amount of the heating energy gets lost due to unwanted heat exchange with the environment. High voltage activation pulses result in faster actuation time, thereby limiting the time frame for any unwanted heat transfer, creating a relatively effective adiabatic heat transfer mechanism. The electric pulses must be short within the micro and millisecond range, depending on the SMA geometry and properties, to prevent any material damage, however.

Motzki et al. [25] reached actuation times in the range of 20 ms and strokes of more than 10% of what the SMA wire length can reach through conventional activation processes. This developed high speed actuation strategy based on short pulses was able to achieve energy savings of up to 80% with respect to the conventional quasi static action strategies. Figure 11 shows the total energy consumption for different SMA wire dimeters as function of the activation voltage and the activation time. The experimental energy consumption was observed to be lower than the theoretically expected energy consumption by about 6.6%. This decrease was attributed to the lower formation strokes attained due to an incomplete phase transformation. Theoretical approaches fail to account for the increasing austenite start temperature for the phase transformation under mechanical stress. During actuation, mechanical stress is not constant, so the actual energy balance differs from that theoretically obtained. The experimentally defined time interval for adiabatic conditions, however, matched the theoretical one.

The activation system developed by Malka and Shilo [24] was very efficient, compared to that proposed by Barnes et al. [26]. The release mechanism in both experiments was similar, as the deployment force in Malka and Shilo [24] was smaller by a factor of 1.5, but the required displacement was larger by a factor of 2.5. The electric pulse duration, which is a critical parameter for obtaining a high energy efficiency, was 0.25 ms in Malka and Shilo. [24]'s experiment, which allowed for the phase transformation to be completed in 0.4 ms. Barnes et al. [26], on the other hand,

developed his activation system to acquire a pulse duration of 5 ms, which achieved the phase transformation in 3 ms. Likewise, due to the remarkably rapid response of Malka and Shilo [24]'s setup, a difference of more than an order of magnitude in the consumed energy was achieved, as Malka and Shilo [24]'s actuator consumed 10.23 J of energy as compared to Barnes et al. [26]'s 135 J energy consumption.

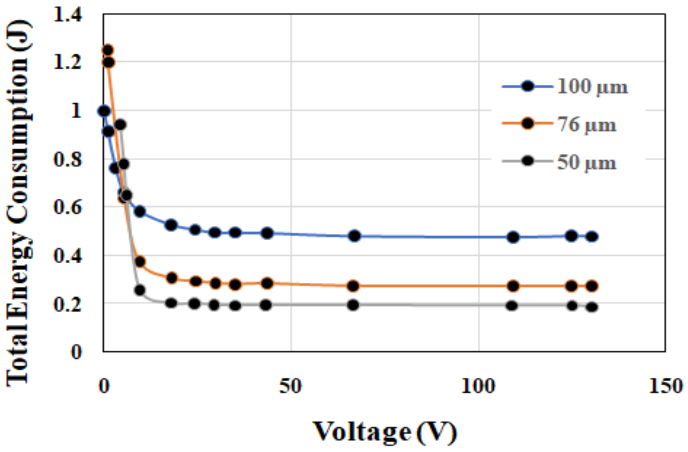

Figure 11. Total Energy consumption for three different SMA wire diameters.

7. Heat transfer modes

Even though inductive resistive heating is the most widely used actuation method due to its ability to execute a fast and homogenous response, thermal actuators can also be used to activate the SME. As previously mentioned, SMA actuation response time is a critical constraint that must be minimized to avoid any limitation to the SMA material's practicality. SMA response time would consist of the heating time required to reach the austinite start temperature and initiate the phase transformation and the SMA material's cooling time [27]. One of the major technical limitations of SMAs are their relatively slow expansion rate when activation using the conventional actuation systems, which is largely attributed to free convective heat transfer to the ambient environment. Since the martensitic phase transformation is an exothermic process, the response time of SMA actuators is dominated by the associated cooling time. This slow cooling time, due to the convective heat transfer limitations, restricts the SMA material's frequency. A thorough assessment and understanding of the heat transfer mechanism is vital to develop a method that effectively increases the cooling rate and reduces the overheating excess power consumption.

A series of strategies can be utilized to mitigate this slow response including maneuver the geometry such that the overall transfer heat is increased, deploying an enhanced heat transfer rate, and finally developing actuation systems independent of the cooling, as in electrical resistance activation using a mechanical latch which is simply deactivated by switching off the current [28]. Likewise, manipulating the heat transfer modes and introducing ones that are efficient can allow us to achieve more practical and cost-effective actuation modes. SMA heat transfer mechanisms can be distinguished as radiation, conduction, and convection. When the enveloping fluid surrounding the SMA material is moving, convection becomes the predominant heat transfer mechanism and

radiation is neglected due to its negligible value. In that case, the heat transfer between an object and ambient is given by Eq 11.

$$P = h \cdot A \cdot \Delta T \tag{11}$$

where P is the transmitted power, h is the heat transmission (convective) coefficient, A is the contact surface area, and ΔT is the difference between the surface temperature and the fixed ambient temperature, usually lower than 100 ^{o}C [29].

The contact surface area can be increased by changing the geometry of the SMA materials to rectangular flat strips rather than round wires or by developing a multiple parallel wire configuration to achieve optimal heat transfer rates. In fact, decreasing the diameter of a wire by half results in a 100% increase in the cooling response time. When the enveloping fluid is stable, not moving, conduction is the predominant method of heat transfer. Conduction is a more effective heat transfer mechanism, as the reported increase in heat transfer rate over free convection lies between a factor of 4 to 10. Similarly, forced convection with highly conductive media has also been reported to allow actuation frequencies greater than 20 Hz.

In 2010, Leary et al. [30] proposed a novel method aimed at decreasing the SMA response time by allowing convective heat transfer through a low-cost lightweight method, consisting of a lagging cylindrical insulation surrounding the SMA wire as shown in Figure 12. The lagging media characteristics and dimensions allow for the manipulation and control of the heat transfer rates. The conductive cooling could be achieved in a production environment by lagging the SMA with a conductive sheath, which has a thermal and geometric properties selected to optimize the response behavior. This electrically insulated conductive sheath would allow the SMA to cool through a conductive mechanism and accommodate the wire contraction by allowing for a varying length and movement associated with the SMA material's behavior.

It was revealed that the repeated actuation results in a lower heating time due to the residual temperature in the lagging system. Likewise, the system reached a steady state response after a series of cyclic loading. The steady state thermal analysis conducted revealed that the total resistance to heat transfer $R_{\text{total}}$is basically a summation of the conductive resistance to the heat transfer of the paste and shell R_{paste} and R_{shell} and the parallel convective and radiative heat transfer to the environment R_{rad} and R_{conv}. Eq 12a–e concludes this finding. Increasing the lagging thickness resulted in an increased resistance to conductive heat transfer and a reduced resistance to convective heat transfer.

$$R_{\text{paste}} = \frac{\ln(r_2/r_1)}{2\pi L k_{\text{paste}}} \tag{12a}$$

$$R_{\text{shell}} = \frac{\ln(r_3/r_2)}{2\pi L k_{\text{shell}}} \tag{12b}$$

$$R_{\text{rad}} = \frac{1}{h_r A} = \frac{1}{2h_r \pi r_3} \approx 0 \tag{12c}$$

$$R_{\text{conv}} = \frac{1}{h_c A} = \frac{1}{2h_c \pi r_3} \tag{12d}$$

$$\begin{aligned} R_{\text{total}} &= R_{\text{paste}} + R_{\text{shell}} + (1/R_{\text{conv}} + 1/R_{\text{rad}})^{-1} \\ &\approx R_{\text{paste}} + R_{\text{shell}} + R_{\text{conv}} \\ &= \frac{\ln(r_2/r_1)}{2\pi L k_{\text{paste}}} + \frac{\ln(r_3/r_2)}{2\pi L k_{\text{shel}}} + \frac{1}{2h_c\pi r_3} \end{aligned} \tag{12e}$$

where L is the thermal resistance per unit length, k is the associated thermal conductivity, h is the heat transfer coefficient, and r_1, r_2, and r_3 are the distances shown in Figure 11.

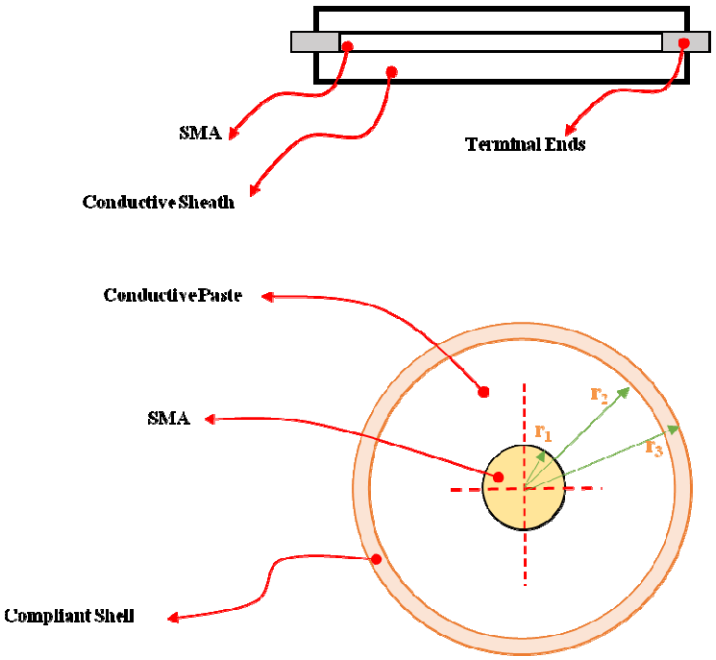

Figure 12. Lagged SMA concept (r_1 refers to the interface between SMA and conductive media, while r_2 refers to the interface between conductive media and the shell, and r_3 refers to the interface between the shell and the ambient environment).

Another important parameter in the mentioned heat transfer method is the critical radius r_{cr}. Cylindrical lagging allows heat transfer resistance to either increase or decrease depending on whether the lagging is greater than or less than the critical length. This critical radius can be utilized to enhance the SMA cooling rate by reducing the total resistance to heat transfer. Figure 13 shows the difference between the lagged and conventional SMA actuator force over time. It is evident that the cooling time associated with the lagged SMA was significantly less than that of the unlagged SMA.

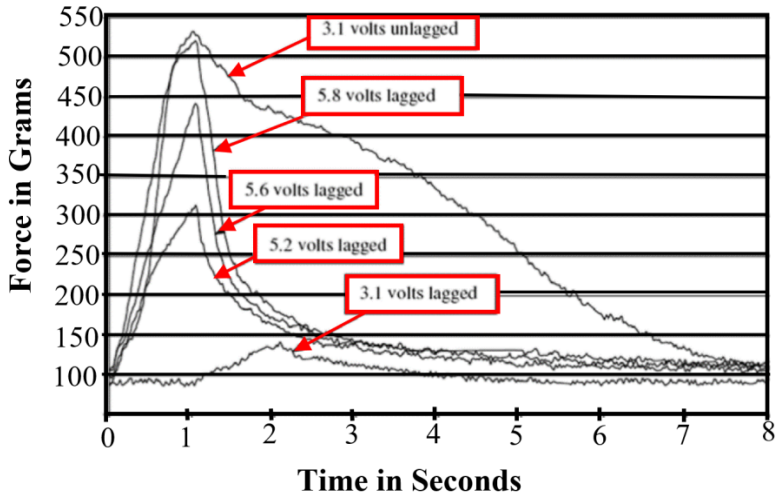

Figure 13. Lagged and conventional SMA actuator force versus time.

An explicit model of the temperature of the SMA material was developed by Huang et al. [31] to determine the temperature time profile during resistive heating. Lagging through direct contact with a highly conductive media was used to reduce the cooling response time to allow a symmetric high-speed activation profile, like that of Leary et al. [30]'s setup. A finite difference equation was devised to predict the associated temperature during the cooling process. The research efforts were focused on utilizing the critical radius associated with concentric layers of thermal material in concert with highly conductive heat transfer media to enhance SMA response time to enhance the SMA materials practicality.

Huang et al. [31]'s initial analysis indicated that the resistive heating time of a bare SMA actuator is remarkably short when compared to the cooling time, and that the proposed lagging method provides a significant opportunity to match that of the heating time. Likewise, it was determined that the minimum observed SMA surface temperature is a critical design objective as it indicates the actuator response time.

The sensitivity analysis assessing the sensitivity of the SMA surface temperature to the associated design variables, like lagging parameters, ambient temperature, and the effects of forced convection, revealed that the shell thickness is an important design variable as the associated conductivity is lower than that of the paste variable. Hence, a larger shell radius resulted in a lower minimum observed SMA temperature than for a smaller shell radius and that the minimum observed SMA temperature associated with a large shell radius is independent of variation to the shell and paste dimensions. Meanwhile, for small lagging radius the effect of shell surface area is dominant over paste conductivity. If any reduction occurs to the shell thickness, it is necessary to maintain the shell radius by increasing the paste radius to prevent compromising the response time.

It must be noted, however, that even though alterations done to an SMA actuation process by changing the convective properties of the cooling medium may result in reducing the SMA material's cooling time, it may result in an increased heat loss and greater power draw during the heating cycle. For instance, for free convection involving basic cooling in still air, the heat transfer mechanism is basic even though the convection heat transfer is low. Adding a fan to improve the air

flow may improve the heat transfer, but this will create a forced convection heat transfer mechanism, which would require additional power draw and system complications [32].

Similarly, even though decreasing the SMA wire diameter or altering the geometry such that the surface to volume ratio is increased and ambient fluid flow is facilitated results in a faster response and lower cooling period, this could decrease the actuator's force output [33]. Understanding such limitations and side effects is critical in gaining an enhanced and thorough insight in the art of dealing with certain imposed demands and requirements. Depending on the application circumstances, one can effectively chose more accurately certain design parameters to develop an optimized actuation scheme.

In 2010, Pathak et al. [34] introduced a non-invasive technique for calculating convective coefficients of SMA via temperature induced transformation strain of the material to estimate the surface temperature. A PVC box was covered to prevent any stray air currents from affecting the free convection in air experiments. On the other hand, the forced convection in air experiment was conducted outside the box, with an electrical fan with a varying proximity and speed to produce a desired test flow rate, which was measured by a hot wire anemometer. The input power was gradually increased, and the recorded power along with the associated ambient and midpoint transformation temperature were used to create empirical correlations that predict the convective coefficient. This provided more accurate estimates of convection, allowing for the optimization of SMA actuators through increased frequency performance while ensuring that the power draw is minimum.

After gathering data for the convective heat transfer in air experiments, it was established that the average convective coefficient over the entire surface of the wire, $\overline{h}$ can be represented by Eq 13.

$$\overline{h} = kC\left(\frac{g\beta(T_s - T_a)}{v\alpha}\right)^m D^{3m-1} \tag{13}$$

where D is the wire diameter, k is the thermal conductivity of the air, C and m are the free variables, g is the acceleration due to gravity, β is the thermal expansion coefficient of the fluid, T_s is the surface temperature of the wire, T_a is the ambient temperature of the fluid, v is the kinematic viscosity of the fluid, and α is the thermal diffusivity.

Overall, the convective heat transfer coefficient decreased as the wire diameter increased, theoretically reaching zero at very large diameters, as very large diameter cylinders would restrict convective flow and the primary mechanism of heat transfer would be through conduction across the fluid. However, flow would not be resisted, and the coefficient would increase to a "free-flow" limit at extremely small diameters.

When subjected to forced convection, the h values for the SMA increased with flowrate but demonstrated a similar dependence on diameter as observed under free convection. Eq 14 proposed by Hilpert [35] can be used to predict the average convective coefficient for horizontal cylinders under forced construction.

$$\frac{\overline{h}D}{k} = C\mathrm{Re}_D^m \mathrm{Pr}^{1/3} \tag{14}$$

where Re_D is Reynolds number and Pr is Prandtl number.

Pathak et al. [34] realized that while increasing the air flow rate dramatically improves the convective heat transfer performance, higher frequency applications may require a change in ambient medium since, as providing high air flow rates may require greater fan sizes and an increased power consumption, which would eventually make SMA unpractical option. Due to its higher convective ability and increased electrical resistance, mineral oil could serve as an attractive alternative to air cooling. Pathak et al. [34] decided on conducting an experiment with light viscosity mineral oil as the ambient medium. Even though mineral oil demonstrated a similar trend with other media with respect to wire diameter, as an increase in diameter generally reduces the heat transfer coefficient. The heat transfer coefficient for all diameters in mineral oil was consistently higher when compared to the free convection in air results. Even though mineral oil provided a higher increment in performance, requiring no additional power draw, the price of packaging complexity is greater than any other media, which is problematic in certain applications.

Experiments investigating the heat transfer properties from SMA wires to thermally conductive grease has also been conducted by Pathak et al. [34]. OmegaTherm OT-201 thermally conductive silicon paste was selected due to its very high thermal conductivity, and its electrically insulating properties. The primary mode of heat transfer through this paste is conduction, as high viscosity of this paste does not flow to produce free convection. Thermal grease was found to provide significantly higher cooling rates for higher frequency responses for a given diameter. However, its increased viscosity decreases the pastes workability, and its expensiveness makes it impractical for large scale applications. Eq 15, based on Morgan [32]'s free convection equation, can be used to predict the average convective heat transfer coefficient, $\overline{h}$:.

$$\overline{h} = Ck[gR(T_s - T_\infty)]^m D^{3m-1} \tag{15}$$

where the fluid properties are lumped into one variable, $R = \left(\frac{\beta}{\nu\alpha}\right)$.

Water immersion was also tested as a possible ambient fluid condition, and the cooling performance for distilled water was tested to be the highest among all media studied. This technique is an effective and simple cooling method that provides protection against overheating if the transition temperature of the SMA material is below the water boiling point. Running excess current through the wires would cause the water to eventually boil, thereby dissipating the extra heat without damaging the SMA material. If the SMA material's transition temperature is higher than the boiling temperature of pure water, additives such as ethylene glycol could be added to raise the fluid's boiling temperature, although this could compromise some of the water's convective properties.

8. Material fatigue and behavior

The cyclic loading behavior of SMA materials, is usually associated with a functional and structural fatigue that directly affects the material's service life. This fatigue is a multiple parameter phenomenon that can be affected by temperature, microstructure, surface quality, and stress/loading asymmetry. Microstructural damage accumulated during cyclic loading results in structural fatigue failure. The stability of the stress strain hysteresis behaviour of SMA during strain-controlled fatigue loading is highly dependent on the material's microstructure. Functional fatigue involves a decrease

in the functional properties, such as work displacement and contraction ability of the SMA and its energy dissipation characteristics. The deterioration of energy dissipation characteristics arises from the gradual change in the SMA microstructure due to fatigue [36].

At ambient temperature, SMA actuators are in their martensitic state. After pseudoplastic deformation beyond, the external force causing this deformation will result in the growth of certain martensitic variants resulting in the elongation of the SMA. When SMA is heated above the austenite start temperature and towards the austenite finish temperature, it contracts. The external load affects the transformation temperatures in this process, and eventually stabilizes the martensitic phase. The microstructure of the material and its chemical composition have a great effect on this thermal cycling and the hysteresis behavior. In fact, the increase in dislocation density during thermal cycling affects the SMA material's functional properties. This functional fatigue arising from the increase in thermo mechanical cycles results in an evident shape recovery loss.

Costanza et al. [37] investigated the shape recovery of nitinol based SMA upon the application of up to 6×10^5 thermo-activation cycles. By applying an 3 V current across the SMA specimen and then disconnecting the power supply for 30 s to cool the SMA down, they were able to monitor the trend between the SMA specimen's maximum extended length and the applied heating cycles, enabling the qualitative assessment of the degradation of the shape memory effect. As seen in Figure 14, the maximum length recoverable by the sample decreases as the number of thermal cycles increases, until eventually reaching a plateau. After analyzing Costanza et al. [37]'s data, Eq 16 to describe this phenomenon.

$$L_{max} = 97.67N^{-0.419} \tag{16}$$

where L_{max} is the SMA specimen's maximum extended length and N is the number of activation cycles applied.

Similarly, the dynamic behaviour of nitinol SMA has been studied using IR thermography to analyze the relationship between the transformation temperatures and thermal cycles, and it has been observed that the temperature required for a phase change gets shifted to a higher temperature as the number of cycles increases, resulting in a functional fatigue deterioration.

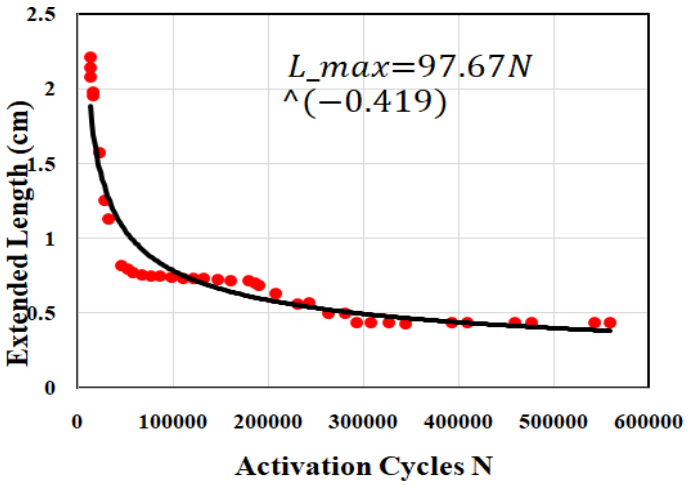

Figure 14. Maximum length vs. number of activation cycles.

Dolce and Cardone [38] investigated the suitability of NiTi SMA wires for seismic applications through a series of cyclic tensile tests. The experimental results showed that the characteristics of the superelastic wires are well suited for seismic applications, due to the superior recentering and energy dissipation features, the tested material showed considerable dependence on the temperature, loading frequency, and number of cycles. A decrease in energy loss and equivalent damping occurs when temperature is due to the latent heat of transformation, which cannot be dissipated in case of high strain rates. A reduction in energy dissipating capacity occurred when the SMA specimens underwent several loading cycles, increasing the cyclic strain hardening, until reaching a stable behavior, which highlighted the importance of prestaining and training the SMA material to gain a more stable behaviour.

Similarly, Costanza et al. [39] investigated the shape memory effect on NiTi sheets, with respect to the applied constant temperatures, through tensile tests conducted on 4–50 mm by 10 mm SMA specimens with the thicknesses shown in Table 1. Even though the material's ability to react to thermal signals deteriorates through fatigue, the experimental data led to the conclusion that fundamental parameters such as the young's modulus, maximum stress, and the ability to recover the original shape increases as temperature increases, and hence, energy dissipation. Figure 15, developed from Costanza et al. [39]'s experimental data, shows the variation of energy dissipation with temperature.

Table 1. Specimen thickness.

Specimen ID	Thickness (mm)
Specimen 1	1.1
Specimen 2	0.5
Specimen 3	0.5
Specimen 4	1

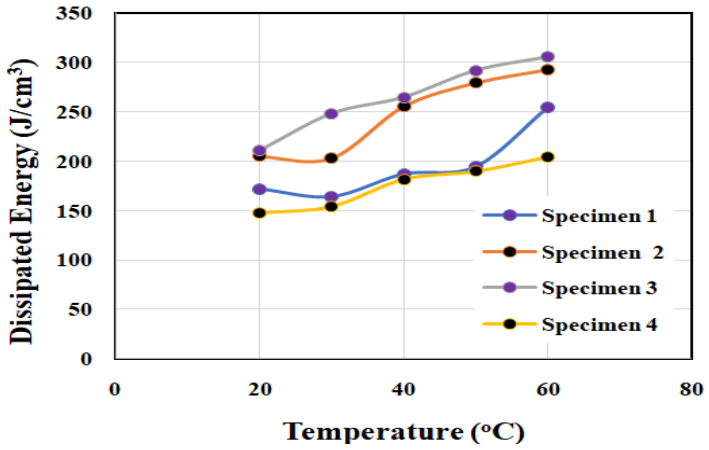

Figure 15. Variation of dissipated energy per material volume with respect to temperature.

9. Conclusion

Shape memory alloys have many great applications and potential that will remain untapped if its limitations regarding activation time and heat transfer are not dealt with. For such limitations to be

treated, one must develop a deep and thorough understanding of the material's characteristics and the different activation techniques associated with it. Certain applications require rapid SME stimulation, hence rapid pulse electro-resistive activation may be used instead of the simple conventional methods. The required input energy can be determined through electro resistive relationships, depending on the requirements of the given application. This allows for an efficient circuit design that meets the needs of the manufacturer.

Likewise, understanding the heat transfer mechanisms and the advantages and drawback each mechanism has on the shape memory alloy behavior is essential to develop an effective SMA system. Manipulating the heat transfer rates to develop an efficient and conservative thermal transition mechanisms through lagging and insulating mediums allows the optimization of SMA actuators. Empirical correlations allow the accurate prediction of convective coefficients, which would allow us to design for enhanced frequency performance while minimizing the power draw. Such a vivid understanding of shape memory alloys would allow a successful optimization of any system utilizing the material.

Finally, understanding the cyclic loading behavior of SMA, considering fatigue behavior is vital in anticipating the behavior of the system utilizing the SMA material, and thereby, determining the suitability of SMA in the given application. Experimental data obtained from cyclic loadings aimed at exploring the fatigue behavior of SMA can help us in developing constitutive models that would allow the evaluation of important mechanical properties after experiencing functional and structural fatigue.

Acknowledgements

The authors are grateful for the financial support provided by the Natural Sciences and Engineering Research Council of Canada (NSERC).

Conflict of interests

The authors declare that they have no conflict of interest.

References

1. Lagoudas DC (2008) *Shape Memory Alloys: Modeling and Engineering Applications*, Springer Science & Business Media.
2. Bunget G (2011) BATMAV—A bio-inspired micro-aerial vehicle for flapping flight [PhD's Dissertation]. USA: North Carolina State University.
3. Duerig T, Stoeckel D, Johnson D (2002) SMA—smart materials for medical applications, *European Workshop on Smart Structures in Engineering and Technology*, Society of Photo-Optical Instrumentation Engineers, 7–15.
4. Kohl M, Popp M, Krevet B (2004) Shape memory micromechanisms for microvalve applications, *Smart Structures and Materials 2004: Active Materials: Behavior and Mechanics*, Society of Photo-Optical Instrumentation Engineers, 106–117.
5. Lan CC, Yang YN (2009) A computational design method for a shape memory alloy actuated compliant finger. *J Mech Design* 131: 021009.

6. Stepan LL, Levi DS, Carman GP (2005) A thin-film nitinol heart valve. *J Biomech Eng-T ASME* 127: 915–918.
7. Veeramani AS, Buckner GD, Owen SE, et al. (2008) Modeling the dynamic behavior of a shape memory alloy actuated catheter. *Smart Mater Struct* 17: 015037.
8. Epps JJ, Chopra I (2001) In-flight tracking of helicopter rotor blades using shape memory alloy actuators. *Smart Mater Struct* 10: 104–111.
9. Gravatt LM, Mabe JH, Calkins FT, et al. (2010) Characterization of varied geometry shape memory alloy beams, *Industrial and Commercial Applications of Smart Structures Technologies 2010*, Society of Photo-Optical Instrumentation Engineers, 7645U.
10. Costanza G, Tata ME (2020) Shape memory alloys for aerospace, recent developments, and new applications: A short review. *Materials* 13: 1856.
11. Abou-Elfath H (2017) Evaluating the ductility characteristics of self-centering buckling-restrained shape memory alloy braces. *Smart Mater Struct* 26: 055020.
12. Carreras G, Casciati F, Casciati S, et al. (2011) Fatigue laboratory tests toward the design of SMA portico-braces. *Smart Struct Syst* 7: 41–57.
13. McCormick J, DesRoches R, Fugazza D, et al. (2007) Seismic assessment of concentrically braced steel frames with shape memory alloy braces. *J Struct Eng* 133: 862–870.
14. Moradi S, Alam MS, Asgarian B (2014) Incremental dynamic analysis of steel frames equipped with NiTi shape memory alloy braces. *Struct Design Tall Spec* 23: 1406–1425.
15. Indirli M, Castellano M, Clemente P, et al. (2011) Demo-application of shape memory alloy devices: The rehabilitation of the S. Giorgio Church bell-tower, *Smart Structures and Materials 2001: Smart Systems for Bridges*, *Structures*, *and Highways*, Society of Photo-Optical Instrumentation Engineers, 262–272.
16. Castellano M, Indirli M, Martelli A (2001) UProgress of application, research and development and design guidelines for shape memory alloy devices for cultural heritage structures in Italy, *Smart Structures and Materials*, Society of Photo-Optical Instrumentation Engineers, 250–261.
17. Croci G (2001) Strengthening of the basilica of St francis of assissi after the September 1997 earthquake. *Struct Eng Int* 8: 56–58.
18. Andrawes B, Shin M, Wierschem N (2010) Active confinement of reinforced concrete bridge columns using shape memory alloys. *J Bridge Eng* 15: 81–89.
19. Hussain MA, Driver RG (2005) Experimental investigation of external confinement of reinforced concrete columns by hollow structural section collars. *ACI Struct J* 102: 242–251.
20. Krstulovic-Opara N, Thiedeman PD (2000) Active confinement of concrete members with self-stressing composites. *ACI Mater J* 97: 297–308.
21. Schmidt M, Ullrich J, Wieczorek A, et al. (2016) Experimental methods for investigation of shape memory based elastocaloric cooling processes and model validation. *JoVE* 111: e53626.
22. Vollach S, Shilo D (2010) The mechanical response of shape memory alloys under a rapid heating pulse. *Exp Mech* 50: 803–811.
23. Vollach S, Shilo D, Shlagman H (2016) Mechanical response of shape memory alloys under a rapid heating pulse-part II. *Exp Mech* 56: 1465–1475.
24. Malka Y, Shilo D (2017) A fast and powerful release mechanism based on pulse heating of shape memory wires. *Smart Mater Struct* 26: 095061.
25. Motzki P, Gorges T, Kappel M, et al. (2018) High-speed and high-efficiency shape memory alloy actuation. *Smart Mater Struct* 27: 075047.

26. Barnes B, Brei D, Luntz J, Browne A, et al. (2006) Panel deployment using ultrafast SMA latches, *ASME 2006 International Mechanical Engineering Congress and Exposition*, 273–280.
27. Huang W (2002) On the selection of shape memory alloys for actuators. *Mater Design* 23: 11–19.
28. Leary M, Schiavone F, Subic A (2010) Lagging for control of shape memory alloy actuator response time. *Mater Design* 31: 2124–2128.
29. Van Humbeeck J (1999). Non-medical applications of shape memory alloys. *Mater Sci Eng A-Struct* 273: 134–148.
30. Leary M, Schiavone F, Subic A (2010) Lagging for control of shape memory alloy actuator response time. *Mater Design* 31: 2124–2128.
31. Huang S, Leary M, Ataalla T, et al. (2012) Optimisation of Ni–Ti shape memory alloy response time by transient heat transfer analysis. *Mater Design* 35: 655–663.
32. Morgan VT (1975) The overall convective heat transfer from smooth circular cylinders, In: Abraham JP, Gorman JM, Minkowycz WJ, *Advances in Heat Transfer*, Elsevier, 11: 199–264
33. Shahin AR, Meckl PH, Jones JD, et al. (1994) Enhanced cooling of shape memory alloy wires using semiconductor "heat pump" modules. *J Intel Mat Syst Str* 5: 95–104.
34. Pathak A, Brei D, Luntz J (2010) Transformation strain-based method for characterization of convective heat transfer from shape memory alloy wires. *Smart Mater Struct* 19: 035005.
35. Hilpert R (1933) Correlations for laminar forced convection in flow over an isothermal flat plate and in developing and fully developed flow in an isothermal tube. *Forsch Ingenieurwes* 4: 215–224
36. Eggeler G, Hornbogen E, Yawny A, et al. (2004) Structural and functional fatigue of NiTi shape memory alloys. *Mater Sci Eng A-Struct* 378: 24–33.
37. Costanza G, Paoloni S, Tata ME (2014) IR thermography and resistivity investigations on Ni–Ti shape memory alloy. *Key Eng Mater* 605: 23–26.
38. Dolce M, Cardone D (2001) Mechanical behaviour of shape memory alloys for seismic applications 1. Martensite and austenite NiTi bars subjected to torsion. *Int J Mech Sci* 43: 2631–2656.
39. Costanza G, Tata ME, Libertini R (2016) Effect of temperature on the mechanical behaviour of Ni–Ti shape memory sheets, *TMS 2016 145th Annual Meeting & Exhibition*, Springer, Cham, 433–439.

AIMS Press